Flow field characteristics of an axisymmetric sudden-expansion pipe flow with different initial swirl distribution

A. S. Nejad and S. A. Ahmed
Experimental Research Branch, Wright-Patterson AFB, Dayton, OH, USA

The results of an experimental investigation depicting the effects of swirl profile on confined flows in a sudden-expansion coaxial dump combustor are presented. Three swirlers (free vortex, forced vortex, and constant angle) with the same nominal swirl number were designed and fabricated to study the effects of swirl type on the isothermal dump combustor flow field. Imparting swirl to the inlet flow resulted in a considerable reduction of the corner recirculation length, a marked increase in turbulent mixing activity, and in one case creation of a central recirculation zone. This article highlights the importance of the combustor inlet swirl profile and shows that swirl type as well as swirl strength can affect the flow field significantly. The present database is well suited for numerical codes development and validation.

Keywords: turbulent; recirculation; swirling; dump combustor

Introduction

Turbulent swirling flows have been and continue to be of considerable interest to both engineers and scientists. The designers of combustion chambers have used swirl to promote rapid mixing of fuel and oxidizer, to enhance flame stabilization, to broaden the combustor operational limits, and to reduce the formation of pollutants and particulates. For analysis of combustion processes, one requires a broad knowledge of interrelated subjects such as injection, atomization and mixing, flow separation and recirculation, ignition, combustion, and heat release. This has made realistic simulation and solution of swirling recirculating turbulent flows a difficult and a challenging task. A considerable number of attempts have been made to model turbulent reacting and nonreacting swirling flows. So far, the efforts have not been always successful. This is due to the problems associated with closure models representing turbulence and chemical reaction. It is generally agreed that the impediments to the development of a mathematical model for flows of engineering interest are the lack of in-depth understanding of turbulence and the applications of inadequate physical models. Today, one of the most commonly used turbulence models for representing isothermal flows is the K-ε two-equation model. For combusting flows, derivatives of the isothermal physical models are used, which may include a simple representation of flame–turbulence interaction. These models have been successful in the simulation of a few relatively simple isothermal and combusting turbulent flows. However, experiments and calculations of the exchange coefficients from mean value distributions have shown that, for swirling flows, the turbulent stress distributions are anisotropic, and the extension of closure models based on a uniform transport mechanism most often fails to predict the flow field accurately. Currently, computational fluid dynamics (CFD) codes suffer from the lack of a proper validation procedure; complementary experimental and analytical studies must be pursued to strengthen combustor design methodology based on CFD. Consequently, a considerable aid to the development of mathematical modeling is the creation of an extensive detailed experimental database that can be used for validations of numerical codes.

Experimental investigations of swirling confined flows have been reported extensively in the past. A swirl velocity, also known as the tangential component, is imparted to the flow by a variety of different techniques such as the use of rotating pipes, tangential inlet-port entries, or axial flow swirlers (flat and curved vane). Swirling flows are usually categorized by the strength or degree of swirl (swirl number S), which is defined as the ratio of the axial flux of angular momentum to the axial flux of the axial momentum (see Equation 1). However, swirl number is not an all-inclusive parameter that can be used to classify the effects of the inlet swirl on the flow field, as will be shown later. The type, the method of generation, and the distribution of the initial inlet-swirl profile significantly contribute to the development of the combustor flow field and must be specified.

The studies of Lilley et al. (1975, 1976, 1977, 1982, 1985) and Gupta et al. (1984, 1985) are some of the famous work in this field. Both experimental and analytical efforts have been reported for flows with varying degrees of swirl. These efforts showed the effects of swirl on the main features of sudden-expansion pipe flow such as the corner recirculation zone (CRZ) and the central toroidal recirculation zone (CTRZ). For weak swirl, the normal stresses were found to be nearly isotropic, with large-scale turbulent structures occurring in the recirculation zones and small-scale turbulence confined to the high-velocity regions of the flow. Measurements farther downstream from the dump plane showed a relatively uniform radial distribution of velocity and low levels of turbulence. Unfortunately, the majority of Lilley's experimental data was obtained

Address reprint requests to Dr. Ahmed at the Experimental Research Branch, Wright-Patterson AFB, Dayton, OH 45433, USA.

Received 5 November 1991; accepted 19 April 1992

by utilizing hot-wires and/or five-hole pitot probes, which can significantly alter the flow field of interest and render the data unsuitable for validation of CFD codes.

Ramos and Somer (1985) used a two-color laser Doppler velocimeter (LDV) to obtain data in a swirling research combustor consisting of two confined concentric swirling jets whose mass flows and swirl numbers were controlled independently. Although their combustor was designed for premixed and nonpremixed reactive flow operations, only isothermal results were reported for both coswirl and counterswirl flow conditions. They compared their results with other experimental data and with numerical results that were obtained using two-equation turbulence models. Contrary to the findings of Vu and Gouldin (1982), it was shown that under both flow conditions a closed recirculation zone was created at the combustor centerline. Since their experimental data did not agree with other experimental data under coswirl conditions, they concluded that swirl number should not be considered to be the only parameter that characterizes swirling flows and that the inlet-flow boundary conditions should also be specified in future experiments. The isothermal experiments of Vu and Gouldin (1982) were similar to the work of Ramos and Somer (1985). Mean flow measurements were obtained for five different flow conditions to determine the effects of outer swirl on the central recirculation zone. They reported that the size and the velocity of the central recirculation zone decreased to zero as the outer swirl magnitude was reduced from maximum counterswirl to coswirl conditions. Surprisingly, the initial velocity profiles were not symmetric. This may have been caused by the intrusive nature of Ramos and Somer's (1985) measuring instrument. They also presented spectral data that revealed periodic oscillations in both flows. Apparently, the oscillations originated from the inner jet, with fundamental frequencies comparable to the rotational frequency of the inner jet. Ramos and Somer (1985) believed that the swirling flow oscillations contribute significantly to higher fluctuation levels in the central regions of the flow. These oscillations have a significant effect on flame stability and on the mixing processes in the shear-layer regions.

Sislian and Cusworth (1986) performed measurements in an isothermal strong swirling free jet, with a single-component LDV system, to provide the three mean-velocity and the six turbulent stress tensor components for turbulence-closure model validation. Their results showed that the normal shear stresses were not isotropic and were significantly larger than the Reynolds shear stresses, as will be explained below. Gouldin et al. (1985) reported data for reacting and nonreacting swirling flows generated by two concentric confined jets. Radial profiles of estimated Favre mean velocity and Favre root mean square (RMS) velocity fluctuations were presented. A closed central recirculation zone was observed for both the coswirl and counterswirl flow conditions in the presence of combustion. For the nonreacting case, only the counterswirling flow produced a central recirculation zone. Large anisotropic velocity fluctuations were observed in the high-shear regions and in the vicinity of the recirculation zone.

Kilik (1985) examined the effects of swirl vane curvature on a combustor flow field. The performance of flat vane swirlers was compared with that of corresponding curved vane swirlers for swirl numbers $S = 1.04$, 1.51, and 2.40. The study indicated that increasing the vane outlet angle from 50° to 70° increased the size of the recirculation region for both the curved and flat vane swirlers. His measurements showed a 50 percent improvement in the combustor pressure recovery by using curved vanes for the same vane outlet angle. In addition, the central recirculation region became larger and stronger, implying that stronger swirl was imparted to the flow at the swirler exit.

Different techniques for swirl generation have been employed by various investigators (see Table 1). These studies covered a wide range of flow and design parameters. The results showed disparity between studies. For example, Keer and Fraser's (1967) method of swirl generation, $S = 0.72$, failed to produce a recirculation zone, while Chigier (1967), employing a different technique, achieved recirculation at a lower swirl number, $S = 0.66$. Most likely, the method of swirl generation, which has not received much attention in the past, can also be a major influencing factor. To illustrate the effects of the initial swirl distribution on the flow field of a free jet, Farokhi et al. (1989) performed experiments with two extreme tangential velocity distributions (i.e., one with a solid-body rotation and the other predominated by a free-vortex distribution). They found that the free-vortex flow distribution was on the verge of vortex breakdown at $S = 0.48$, a phenomenon associated with higher swirl number flows, i.e., $S_{crit} > 0.6$. They concluded that the integrated swirl parameters, such as the swirl number, may not be adequate in describing the near field flow characteristics. Similar to this, the present experiments were conducted to study the effects of inlet swirl profile on the combustor flow field. For this purpose, three swirlers (free vortex, forced vortex, and constant angle) with the same nominal swirl numbers, $S = 0.4$, were designed and fabricated. Detailed measurements of the velocity field of a typical dump combustor with and without these inlet swirlers are conducted.

Notation

C_p	Pressure coefficient, $C_p = (P_{is} - P_w)/(P_t - P_{is})$
H	Step height
K	Turbulent kinetic energy
L	Length of corner recirculation zone
M_u	Normalized axial momentum
M_w	Normalized tangential momentum
r	Radial coordinate
R	Combustor radius
S	Swirl number
U, V, W	Time mean axial, radial, and tangential velocities
u', v', w'	RMS turbulent axial, radial, and tangential velocities
$\overline{uv}$	Reynolds shear stress (U-V plane)
$\overline{uw}$	Reynolds shear stress (U-W plane)
X	Axial distance from the dump plane

Greek symbols

ΔP	$P_{X@18} - P_{X@0.38}$
ΔM	$M_{u,X@18} - M_{u,X@0.38}$
σ	Standard deviation

Subscripts

i	Inlet pipe
is	Inlet static value
o	Zero swirl
ref	Inlet centerline value upstream of the swirler
t	Inlet stagnation value
w	Combustor wall
c	Centerline values

Table 1 Summary of experimental methods for swirl generation

Author	Method	Measurement	Swirl no.	Recirculation
Rose, 1962	Rot. pipe	Hot-wire	0–0.23	No
Chigier, 1964	Tan. ports	Impact probe	0.30–1.43	Yes
Kerr, 1965	Vanes	Impact probe	0–0.72	No
Chigier, 1967	Tan. ports	Impact probe	0.13–0.66	Yes
Mathur, 1967	Vanes	Impact probe	0–2.7	Yes
Maier, 1975	Vanes	Impact probe	1.7–2.9	Yes
Craya, 1967	Tan. ports	Hot-wire	0–1.58	Yes
Syred, 1971	Tan. ports	Hot-wire	2.2	Yes
Pratte, 1972	Rot. pipe	Hot-wire	0.3	No
Hosel, 1979	Tan. ports	LDA	0–1.7	Yes
Fornoff, 1978	Tan. ports	LDA	0.53	No
Riberio, 1980	Tan. ports	Hot-wire	0.32	No

Experimental setup

Combustor facility

The present experiments were conducted in the same flow facility described in detail by Nejad et al. (1989) and Favaloro et al. (1991) (see Figure 1). The flow facility was designed to allow easy insertion and change of swirlers. Also, it provided easy access to the inside of the combustor for cleaning of the optical view ports. The flow model consisted of two major sections, the inlet pipe (2850 mm in length and 101.6 mm inner diameter (ID)) and the combustor chamber (152.4 mm ID and 1850 mm in length). The inlet pipe, containing pressure and temperature instrumentation for monitoring the inlet flow, was bolted to the Teflon swirler housing (104.5 mm ID, 152.4 mm outer diameter (OD), and 154 mm in length) to allow swirler replacement. The combustor chamber was constructed from a Plexiglas pipe that terminated in a large rectangular Plexiglas chamber (1210 × 890 × 890 mm) to aid in flow visualization studies. Pressure taps were located at 25.4-mm intervals over the entire span of the combustor. A unique feature of the design was the ability of moving the dump plane relative to the measurement station (38 × 38-mm window). This eliminated the requirement for a flat window covering the span of the combustor. The swirlers used in this study were free-vortex, constant-angle, and forced-vortex swirlers. Each one had 12 circular arc inlet guide vanes welded between a 101.6-mm outer ring and a 19-mm central hub, as shown in Figure 1. The swirl vane geometry was designed by Buckley et al. (1983). All swirlers had nominal swirl numbers of 0.4 calculated assuming uniform

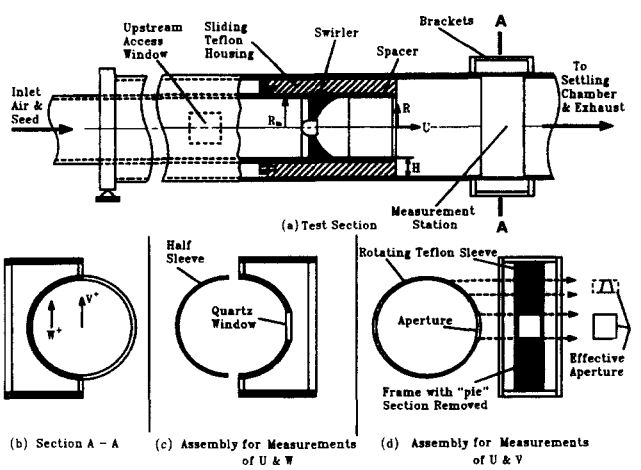

Figure 1 Schematic of the dump combustor flow model

axial velocity distribution on both sides of the swirler. However, it was noted that the actual swirl number as defined by Equation 1 differed from the nominal design value to be discussed later in this article.

$$S = \int_0^R UWr^2 dr \Big/ \int_0^R RU^2 r dr \qquad (1)$$

Throughout this study, the swirler exit plane was located 50.8 mm upstream of the dump plane. Swirlers were replaced by a spacer for studies without inlet swirl.

Laser velocimeter

A two-color, four-beam LDV system was used for velocity and turbulence measurements. The system operated in the back-scatter mode and consisted of two Bragg cells, a 3.75X beam expander with 35-mm beam entrance separation, and a final focusing lens 178 mm in diameter with a focal length of 450 mm. The blue and green lines of an Argon ion laser operating at 300 mW were used in all measurements. To provide directional sensitivity and to remove fringe bias, both sets of fringes were frequency shifted at 40 MHz. The optical system was configured so that the fringe inclination with respect to the horizontal plane was at 45.667° and 135.167°. The sizes of the final probe volumes, based on $1/e^2$ intensity points, were roughly 60 microns in diameter and 600 microns in length, with a fringe spacing of approximately 1.8 microns. The entire optical system was mounted on a three-axis traversing system.

To seed the flow, the chemical seeder of Craig et al. (1986) was used. The seeds were injected in the low-pressure side of the centrifugal blower to achieve uniform particle density. With this configuration, it was possible to achieve 5,000–10,000/s validated (16 fringe counts at 1-percent comparison setting) data rates. The subsequent coincidence data transfer rate ranged from 2,000–5,000/s, with the implementation of a 20-msec coincidence window.

Data acquisition and analysis

Doppler signals from the photomultipliers were processed by two TSI burst counters, Models 1990 B&C with low- and high-pass filters set at 100 MHz and 20 MHz, respectively, on each processor. To reduce statistical uncertainties in the calculation of the higher-order moments of turbulent fluctuations, 27,300 realizations per channel were collected at each measurement location. Data transfer to the dedicated Mod-Comp computer system was accomplished in DMA mode, at a maximum rate of one megabyte per second, through a custom-made interface. Double-precision (48-bit) calculations

of all statistical moments using standard formulas were made at each measurement location. In most cases, the data were sufficiently noise-free to avoid the use of cut-off limits (within the three sigma rule) on the calculated velocity histograms.

The problem of velocity bias in LDV measurements has been examined thoroughly by many investigators. This error arises from the fact that counter-type signal processors make discrete velocity measurements from individual realizations of seed particles passing through the measurement volume. In a uniformly seeded flow, the number of particles per unit time passing through the measurement volume is proportional to the flow rate through that volume, and simple arithmetic averaging of an ensemble of realizations will produce results biased toward values greater than the true temporal mean. This effect is more pronounced in highly turbulent flows, and a number of different schemes have been proposed for its removal. The method adopted in the current study used the time between individual realizations (particle interarrival time) as a weighing factor (see Nejad et al. 1989) for bias correction. The uncertainty of the measured mean velocities was determined using the techniques described by Synder et al. (1984). The uncertainty "ΔU" is determined by the following relation:

$$\Delta U = \pm 1.96 S_u / \sqrt{N} \tag{2}$$

For 95-percent confidence level, the constant 1.96 is used; S_u is an estimator for the true standard deviation; and N is the sample size. From the above relation, the maximum uncertainties of the mean quantities (i.e., U, V, W) due to random errors were found to be 0.4, 0.35, and 0.35 percent of the upstream centerline velocity, respectively.

Results and discussion

The present investigation is part of an ongoing work to characterize the flow in a coaxial sudden-expansion dump combustor with and without combustion. The results of isothermal flows with three swirlers along with that of a simple dump are presented herein. The LDV measurements made in the horizontal and vertical planes provided a detailed mapping of the flowfield, which is shown in Figures 2 through 9. All data presented are normalized with respect to the inlet centerline velocity, U_{ref}, before the swirler or the appropriate upstream flow parameter. The combustor physical dimensions and the measurement coordinates are normalized with respect to the step height, H.

Inlet flow

The inlet flow was the same as reported earlier by Nejad et al. (1989) wherein the measurements were made in the horizontal plane $3.70H$ upstream of the swirler. The data showed that the flow was quite symmetric, with axial turbulence intensity of 5 percent at the center increasing to 9.5 percent near the wall. As expected, the tangential velocity was negligible. The azimuthal turbulence intensity increased from 4 percent at the center to roughly 8 percent at the wall. Thus, the inlet flow was similar to a fully developed pipe flow with nearly isotropic turbulence. The inlet discharge coefficient was calculated to be 0.85.

Combustor flow

It is beneficial to divide the inlet combustor cross section into three distinct regions based on the behavior of the flow. The first region with uniform velocity is called the core region (CCR).

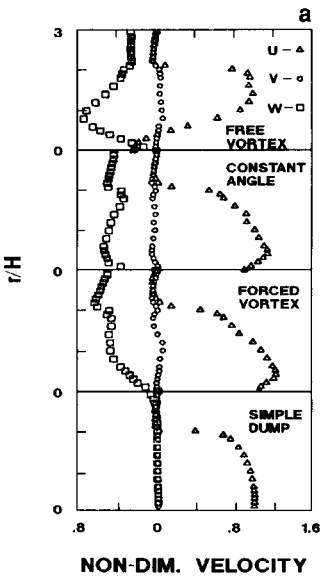

Figure 2a Radial distribution of inlet mean velocity profiles

For example, the core for the zero-swirl case occupied the entire combustor inlet cross section, $0 \leqslant r/H \leqslant 2$. The second region is defined as the combustor wall region (CWR), which is significantly affected by the wall shape or its presence; for example, at the dump plane CWR is large and comparable to the step size. The third region is a mixing region (CMR), which is located between the CCR and CWR. This region can be very small as in the case of the simple dump or can be significantly large as in the case of free-vortex flow.

Figure 2a shows the three components of the velocity field for the four cases studied at $X/H = 0.38$. For all cases studied, the distribution of the radial velocity remained nearly constant, with negligible values as compared to the axial and tangential values. However, the axial velocities behaved considerably differently from each other. The simple dump showed a large CCR that occupied the entire inlet region, $0 \leqslant r/H \leqslant 2$. The corner recirculation region CRZ was confined to the step region, $r/H \geqslant 2.0$. Both the forced-vortex and the constant-angle flows displayed similar axial velocity patterns that consisted of a very narrow CCR, roughly equal to the swirler hub diameter, with minimum and maximum velocities at $r/H = 0$ and $r/H = 0.5$, respectively. Measurements outside of the CCR showed decreasing velocities with negative values for the corner recirculation regions. The free-vortex flow field exhibited an entirely different axial flow pattern. The combustor mixing region is shown to be large with negative velocities in the center depicting the central recirculation zone. Outside of the CMR, measurements showed a very rapid flow deceleration and negative values for the CRZ. As expected, the tangential velocity pattern for the simple-dump case showed insignificant values across the combustor. For the forced- and free-vortex flows, the tangential velocities increased linearly (i.e., solid-body rotation) with increasing radius up to $r/H = 0.8$. After this point, the W-component of the free-vortex flow decreased with increasing radial coordinate up to $r/H = 2$, the point where the step starts, beyond which the azimuthal component stayed constant in the CRZ. In the case of forced-vortex flow, the W-component of the velocity remained nearly constant up to $r/H = 2$, beyond which it increased slightly and decayed gradually in the CRZ. The constant-angle swirler produced a "nearly constant" W-component of the velocity along the radius with a discontinuity at $r/H = 2$.

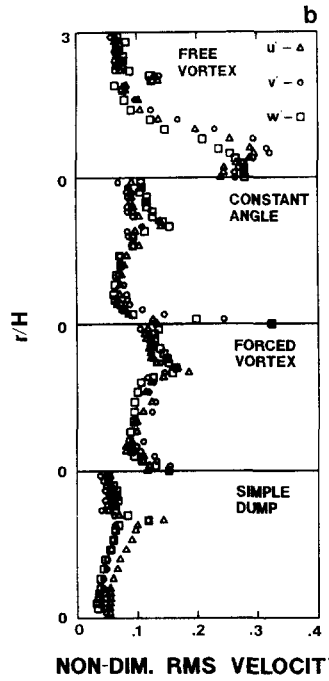

Figure 2b Radial distribution of inlet RMS velocity profiles

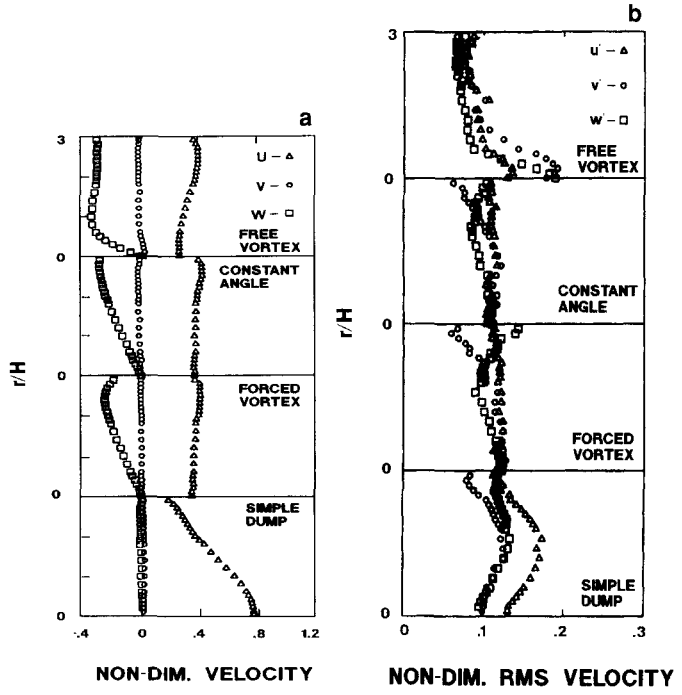

Figure 3a Radial distribution of exit mean velocity profiles

Figure 3b Radial distribution of exit RMS velocity profiles

Turbulence intensity profiles at the combustor inlet, $X/H = 0.38$, are shown in Figure 2b. There are two peaks for the swirling flows; one peak occurred at or near the centerline and the other occurred in the mixing region very close to the separation point at $r/H = 2$. For the simple-dump flow, the data displayed only one peak, which was in the shear layer at $r/H = 2$. The combustor flow field for all cases was not isotropic at the inlet, with anisotropic ratios v'/u' and w'/u', varying between 0.6 to 1.4.

Figures 3a and 3b show the recovery and the redevelopment of the combustor flow field at the combustor exit plane, 18 step heights or three combustor diameters downstream of the dump plane. The axial velocity profiles for the swirling flows showed a nearly complete flow recovery to a flat profile. The free-vortex flow with its large central recirculation region showed small wake effects in the combustor central region. The incomplete recovery of the simple dump, zero swirl, was clearly evident. The radial velocity distribution for all cases showed negligible values throughout the combustor cross section. The swirl behaviors of the forced-vortex and constant—angle swirling flows were as anticipated, with the W-component approaching a solid-body rotation. However, for the free-vortex case, the radial distribution of the tangential velocity field was significantly different. For example, the flow behavior is similar to a forced-vortex flow (i.e., near the centerline while away from the center, the flow displayed constant-angle behavior with a nearly constant tangential velocity component across the rest of the combustor). Similar behavior was observed and reported earlier by Nejad et al. (1989) for a stronger constant-angle swirling flow, $S = 0.5$. It is interesting to note that both the free-vortex flow of the present study and the constant-angle swirling flow of the previous work contained central recirculation regions. On the other hand, a weaker swirling constant-angle inlet flow, ($S = 0.3$), which did not induce a central recirculation zone, behaved in a similar way to the forced vortex. At this point, it is helpful to tabulate the global features of the dump combustor flow field with inlet swirl. Table 2 delineates these features. All parameters have been normalized relative to their corresponding zero swirl values except for the length of the central recirculation zone, which is normalized relative to the step height.

Figures 4a and 4b show the variation of centerline axial velocities and turbulence intensities along the combustor. The simple-dump flow showed a gradual velocity decay, typical of sudden-expansion pipe flows, from a maximum value of $U_c/U_{ref} = 1.0$ at the inlet to 77 percent of the inlet velocity at the combustor exit, $X/H = 18$. Based on an inlet/combustor area ratio of 0.43, and assuming incompressible flow, a flat velocity profile at the combustor exit required the centerline velocity to be roughly 43 percent of the upstream inlet velocity. As evident from the centerline velocity and the velocity profiles shown in Figure 3a, the flow field of the simple dump showed incomplete recovery, with maximum flow velocity occurring at the combustor centerline. Redevelopment of the combustor velocity field with swirl was much more rapid. For all swirlers, the centerline velocity, U_c/U_{ref}, at the combustor exit approached the asymptotic value of 0.43. For example, U_c/U_{ref} was equal to 0.36, 0.35, and 0.29 for constant-angle, forced-vortex, and free-vortex swirlers, respectively. The centerline near field behavior of the forced vortex and the simple dump were similar. Their centerline velocity characteristics began to deviate at $X/H = 3.5$, which roughly coincided with the CRZ reattachment point of the forced-vortex flow. Farther downstream, the decay for the forced-vortex flow was at a much faster rate to show a uniform axial velocity distribution at $X/H = 18$. From the inlet, the constant-angle swirl distribution resulted in very rapid velocity decay. The scatter in the data

Table 2 Global features of dump combustor flow field

Swirl no.	Swirl type	L/L_0	$\Delta P/\Delta P_0$	$\Delta M/\Delta M_0$	L_{ctrz}/H
0.4	CA	0.43	0.63	1.29	0.0
0.4	FOV	0.34	0.71	1.43	0.0
0.4	FRV	0.48	1.04	1.39	7.9

Note: CA = constant angle; FOV = forced vortex; FRV = free vortex

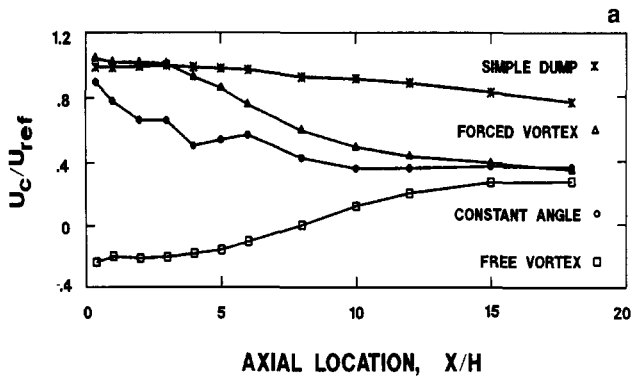

Figure 4a Evolution of centerline axial velocity

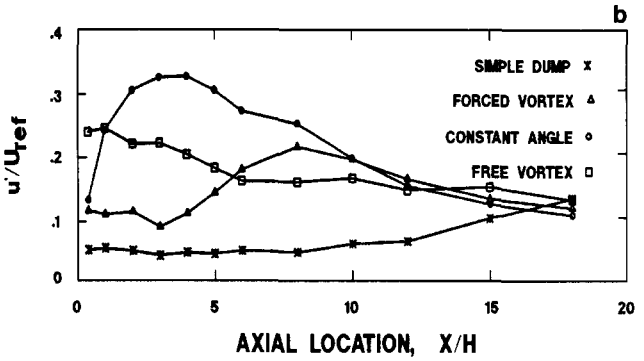

Figure 4b Evolution of centerline axial turbulence intensity

for this case is attributed to the greater unsteadiness of the flow as evident from flow visualization studies. Free-vortex swirl distribution created a very large recirculation region at the center of the combustor, resulting in negative velocity along the combustor centerline up to $X/H = 7.9$. The centerline velocity at combustor exit is lower than the values associated with the other swirlers. This is largely the result of the very large central toroidal recirculation zone, which still manifested itself on the combustor flow field even at the last measurement station, $X/H = 18$. The variations of the centerline axial turbulence intensity distribution along the combustor are shown in Figure 4b. The simple-dump flow showed much lower turbulent activity at the center where the turbulent velocity along the centerline remained nearly constant, $u'/U_{ref} = 0.05$, within the potential core of the flow. It then began to show a moderate increase to reach a maximum level at the combustor exit plane. The axial turbulent velocity for the forced-vortex inlet swirl distribution remained constant up to $X/H = 2$–3, after which it showed a marked increase in turbulent activity, with the peak value $u'/U_{ref} = 0.22$ at $X/H = 8$. At the exit, the centerline turbulence had decayed to show agreement with the other cases. The turbulent activity associated with the constant-angle inlet swirl distribution showed a steep gradient near the dump with a maximum value of $u'/U_{ref} = 0.35$ at $X/H = 3$. Measurements farther downstream showed lower turbulence levels. The intense near field turbulent activity is believed to be the result of the large-scale flow oscillation, precessing vortex, which contributed to the overall statistics of the flow. Turbulence associated with the free-vortex inlet flow showed the highest value at the dump plane, which monotonically decreased with increasing axial distance.

Figure 5 shows the distribution of the turbulent kinetic energy, $K = 0.5(u'^2 + v'^2 + w'^2)$, along the combustor centerline. The trends and the shapes of the curves are similar to the axial turbulence intensity profiles of Figure 4b. The values for the simple dump were the lowest and stayed relatively constant along the combustor. Turbulent transport was not significantly improved by inducing a forced-vortex profile; only a modest improvement over the simple dump was realized. The free-vortex swirler had a more dramatic effect on the ensuing flow field. Ironically, the turbulent activity within the central recirculation zone was not constant (see Figure 2b); it showed a decaying profile, with the maximum and the minimum levels occurring at two and six step heights, respectively. Beyond $X/H = 6$, the turbulent energy level remained relatively constant along the combustor centerline. The turbulent kinetic energy associated with the constant-angle swirl profile was surprisingly the highest. A dynamic central precessing vortex core created large-scale flow oscillations in the radial and tangential directions, which substantially contributed to the overall statistics of the velocity measurements. Flow visualization studies proved that the previous statement is correct, and movies of the flow pattern are available upon request from the authors.

Figures 6a and 6b show the variation of the integrated axial and angular momenta along the combustor at 12 measurement

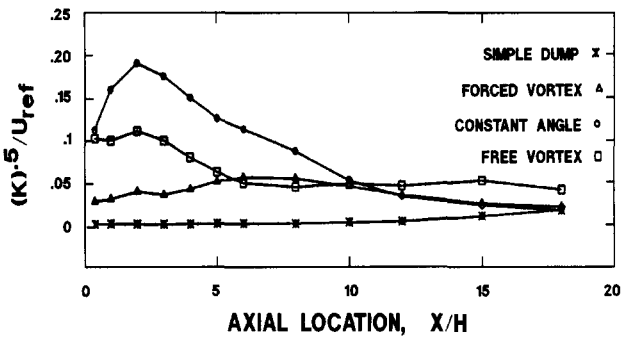

Figure 5 Distribution of axial turbulent kinetic energy

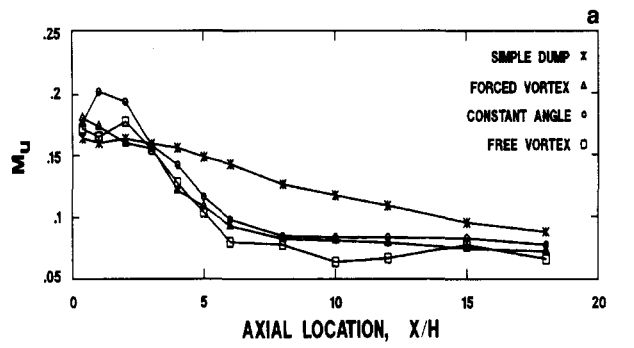

Figure 6a Distribution of axial momentum

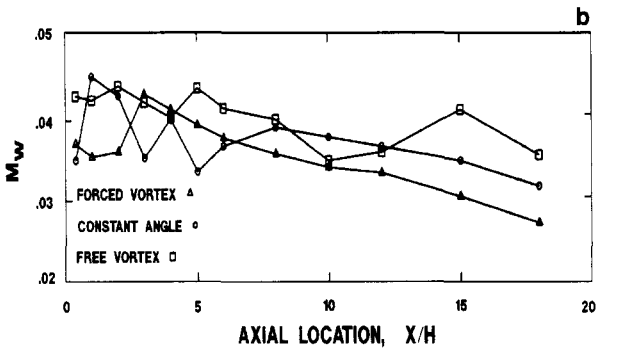

Figure 6b Distribution of angular momentum

stations. The normalized axial and tangential momenta are defined as follows:

$$M_u = \int_0^R (U/U_{ref})^2 r dr/R^2 \quad (3)$$

$$M_w = \int_0^R (UW/U_{ref}^2) r^2 dr/R^3 \quad (4)$$

The decay of axial momentum for the case of simple-dump combustor flow is gradual and monotonic, with the maximum and the minimum occurring at the combustor inlet and exit planes. Inlet swirl profiles drastically modified this decay pattern. Initial momentum loss over the first portion of the combustor ($0.38 \leq X/H \leq 6$) was severe, with all the three flows showing same rate of decay. Beyond $X/H = 6$, which is well past the corner reattachment point of the swirling flows, the axial momentum loss became negligible and the three flows displayed nearly the same magnitude. Figure 6b shows the distribution of the integrated angular momentum for the three swirling flows at the same 12 stations along the combustor. The loss of angular momentum through the combustor was not significant. However, due to the dynamic oscillation of the precessing vortex core and the expanded scale, the results showed some scatter.

All swirlers were designed to produce a nominal swirl number of $S = 0.4$ based on uniform distribution of axial velocity on both sides of the swirler. In practice however, the assumption of downstream flow uniformity is invalid (see Figure 2a). Equation 1 was used to calculate swirl strength for each of the swirlers at the measured axial locations along the combustor, and the results are shown in Figure 7. At or near the dump plane, the swirl numbers were considerably lower than the expected design value. In a short distance downstream of the step, the three flow fields quickly developed to show swirl strengths approximating the design value. From $X/H = 8$ and up to the combustor exit plane, the swirl values for the constant-angle and the forced-vortex inlet flows stayed relatively constant and were nearly equal to the design value. Initially, the swirl strength of the free-vortex flow was slightly lower than expected. However, from $X/H = 5$ to the combustor exit, the flow developed to show stronger swirl than the expected value of $S = 0.4$. It is worth noting that in spite of the large variations along the combustor, for each of the swirlers, the mean swirl strength over the test section approximated the nominal design value. These results are presented in Table 3. A comparison between the data presented in Tables 2 and 3 revealed that the free-vortex swirler with a relatively low initial swirl strength resulted in formation of a central recirculation region. Other investigators did not report recirculation for flows with comparable or much stronger swirl strength. Again, this pointed to the importance of the initial swirl profile, which can strongly influence the characteristics of the combustor flow field.

Table 3 Summary of combustor swirl strength

Swirl type	Design value	Inlet value	Mean value
CA	0.4	0.199	0.332
FOV	0.4	0.205	0.339
FRV	0.4	0.249	0.411

Note: CA = constant angle; FOV = forced vortex; FRV = free vortex

This study has furnished a nearly complete set of velocity and turbulence data that can be used for CFD code validation (i.e., three velocity components and five of the six shear stresses). Measurements in the vertical and horizontal planes have shown the symmetry of the flow field. Note that, since the laser velocimeter in this study was a two-component system, traverses in the vertical and horizontal planes were necessary to realize all three components of the velocity field together with the three normal stresses, two Reynolds shear stresses ($\overline{uv}$, $\overline{uw}$), and seven of the nine triple products, i.e., $\overline{u'^3}$, $\overline{v'^3}$, $\overline{w'^3}$, $\overline{u'^2v'}$, $\overline{u'v'^2}$, $\overline{u'^2w'}$, $\overline{u'w'^2}$. The turbulent transport properties of the flow field will not be discussed in this article. However, the velocity vector plots in the $U-V$ plane (measurements in the vertical plane) are shown in Figure 8. These plots provided a clear quantitative visualization of the four flow fields. Imparting swirl to the combustor inlet flow decreased the length of the CRZ from $8.25H$ for the case of the simple dump to a minimum of $2.8H$ for the forced-vortex flow. Contrary to expectation, the corner recirculation length and swirl strength did not show an inverse relation. The results in Table 3 and Figure 7 show a strong initial and overall combustor swirl strength for the free-vortex swirl profile. Yet, the CRZ length for the free-vortex flow was 42 percent greater than the CRZ length of the forced-vortex flow and was 25 percent larger than the corresponding length of constant-angle swirl distribution. The simple-dump and the forced-vortex swirl generator created similar near field velocity patterns. All swirling flows rapidly recovered and redeveloped to show almost flat axial velocity profiles with a very thin wall boundary layer at the combustor exit plane. This study was designed to neglect the effects of combustor nozzle on the near field, CTRZ and CRZ, and flow behavior. The study of a short coupled combustor-nozzle configuration is important for ramjet applications and must be considered in the future.

Wall static pressure distribution for the cases of no-swirl, free-vortex, constant-angle, and forced-vortex swirl generators

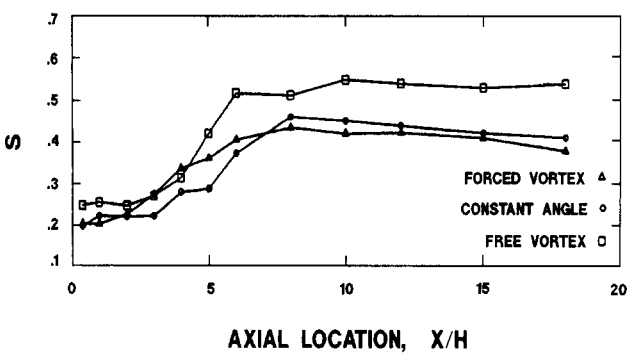

Figure 7 Evolution of swirl strength along the combustor

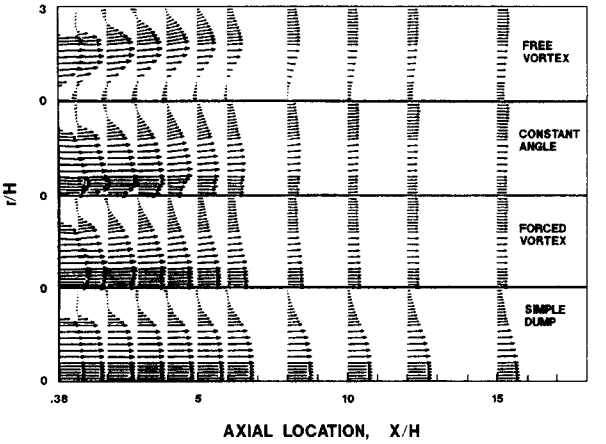

Figure 8 Velocity vector plots ($U-V$ plane)

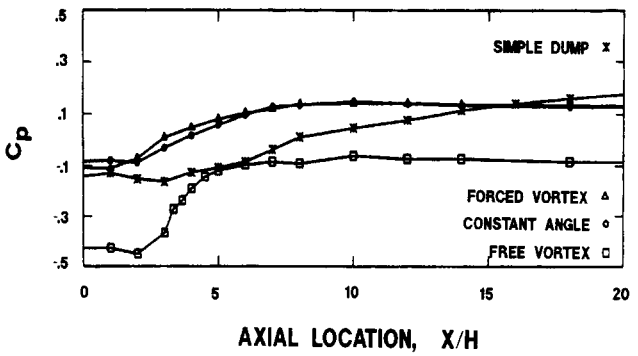

Figure 9 Combustor wall static pressure distribution

is presented in Figure 9. The pressure recovery for the case of no swirl was the slowest where minimum pressure occurred in the corner recirculation region with subsequent monotonic pressure rise throughout the combustor. The pressure loss associated with insertion of these swirl generators was minimal. Combustor pressure recovery for the flows with an inlet swirl generator was much more rapid. For both the constant-angle and forced-vortex swirlers, wall static pressure increased from a minimum value at the dump plane to a relatively constant value (from $X/H = 8$ to the exit). The pressure loss through the free-vortex swirl generator was the largest of the three, as evident from the plot. However, the pressure recovery was the fastest to show a uniform wall static pressure from $X/H = 5$ to the exit plane. This is also observed by others, such as Buckley et al. (1983), who showed that the free-vortex swirler operated at higher combustion efficiencies with a marginally greater combustor pressure loss.

Summary and conclusion

The present experimental effort provided a forum to study the effects of initial swirl distribution on dump combustor flows. Three swirlers of the same nominal swirl strengths with different initial swirl profiles were designed and used. Imparting swirl significantly altered the combustor flow field. In relation to the simple-dump case, the length of the corner recirculation zone was significantly reduced. Only the free-vortex swirl generator was capable of inducing a central recirculation region.

The initial velocity distribution at the dump plane showed significant differences in both the axial and tangential velocity patterns. The flow recovery with initial swirl distribution was quick for all cases and showed a relatively flat axial velocity profile with a very thin wall boundary layer at the exit plane.

The calculated swirl strength based on the distribution of the axial velocity held downstream of the swirl generators showed great deviation from the nominal design value. Contrary to previous studies, the size of the corner recirculation zone and the initial swirl strength did not show an inverse relationship, as expected. Turbulent activity for the constant-angle flow at the combustor centerline was the greatest, which is believed to be the result of large-scale motion of the precessing vortex core.

Acknowledgments

The authors wish to acknowledge the support of the Air Force Office of Scientific Research and Dr. J. M. Tishkoff. Many thanks to Mr. J. Hojnacki for his undivided support. Also, we wish to thank Mr. P. Buckley for his swirlers and for useful discussion.

References

Buckley, P. L., Craig, R. R., Davis, D. L., and Schwartzkopf, K. G. 1983. The design and combustion performance of practical swirlers for integral rocket/ramjets. *AIAA J.*, **21**, 733–740

Chigier, N. A. and Bear, J. M. 1964. Velocity and static pressure distribution in swirling air jets issuing from annular and divergent nozzles. *ASME J. Basic Eng.*, **86**, 788–796

Chigier, N. A. and Chervinsky, A. 1967. Experimental investigation of swirling vortex motions in jets. *ASME J. Appl. Mech.*, **89**, 443

Craig, R. R., Nejad, A. S., Hahn, E. Y., and Schwartzkopf, K. G. 1986. Approach for obtaining unbiased laser doppler velocimetry data in highly turbulent flows. *AIAA J. Propulsion Power*, **2**, 541–545

Craya, A. and Darrigol, M. 1967. Turbulent swirling jet. *Phys. Fluids Suppl., Boundary Layers and Turbulence*, **24**, 197–205

Farokhi, S., Taghavi, R., and Rice, E. J. 1989. Effects of initial swirl distribution on the evolution of a turbulent jet. *AIAA J.*, **27**, 700–706

Favaloro, S. C., Nejad, A. S., and Ahmed, S. A. 1991. An experimental and computational investigation of isothermal swirling flow in an axisymmetric dump combustor. *J. Propulsion Power*, **7**, 348–357

Fornoff, M. 1978. Experimentalle und Theoretische untersuchung von Drallstrahlen. Diplomarbeit, University of Karlsruhe, West Germany

Gouldin, F. C., Depsky, J. S., and Lee, S. L. 1985. Velocity field characteristics of a swirling flow combustor. *AIAA J.*, **23**, 95–102

Gupta, A. K., Lilley, D. G., and Syred, N. 1984. *Swirl Flows.* Abacus Press, Turnbridge Wells, England

Gupta, K. K. and Lilley, D. G. 1985. *Flowfield Modeling and Diagnostics.* Abacus Press, Turnbridge Wells, England

Hosel, W. 1979. Drallstrahlenuntersuchungen mit Einen Weiterentwicketten Lasser Doppler-Messverfahren. Dept. SFB 80/E/120, University of Karlsruhe, West Germany

Kerr, N. M., and Fraser, D. 1965. Swirl, part I: effect on axisymmetric turbulent jets. *J. Inst. Fuel*, **38**, 519–526

Kilik, E. 1985. Better swirl generation by using curved vane swirlers. AIAA Paper No. 85-1087, Reno, NV, 1985

Lilley, D. G. 1985. Swirling flows in typical combustor geometries. Paper AIAA-85-0184, Reno, NV

Lilley, D. G. and Rohde, D. L. 1982. A computer code for swirling turbulent axisymmetric recirculating flow in practical isothermal combustor geometries. NASA CR-3442

Lilley, D. G. 1977. Swirl flows in combustion: a review. *AIAA J.*, **15**, 1063–1078

Lilley, D. G. 1976. Turbulent swirling flame prediction. *AIAA J.*, **14**, 749–756

Lilley, D. G. 1975. Combustor swirl flow modeling. *AIAA J.*, **13**, 419–420

Maier, P. Untersuchung Isothermer Turbulenter Drallfreistrahlen und Turbulenter Drallflammen. Dissertation Thesis, University of Karlsruhe, West Germany

Mathur, M. L. and MacCallum, N. R. L. 1967. Swirling air jets issuing from vane swirlers. Part I: free jets. *J. Inst. Fuel*, **40**, 214–238

Nejad, A. S., Favaloro, S. C., Vanka, S. P., Samimy, M., and Langenfeld, C. 1989. Application of laser velocimetry for characterization of confined swirling flows. *ASME J. Eng. Gas Turbine Power*, **111**, 36–45

Pratte, E. D. and Keffer, J. F. 1972. The swirling turbulent jet. *ASME J. Basic Eng. Ser. D*, **94**, 739

Rose, W. G. 1962. A swirling round turbulent jet. Part I: Mean flow measurements. *ASME J. Appl. Mech. Ser. E*, **29**, 615

Riberio, M. M. and Whitelaw, J. H. 1980. Co-axial jets with and without swirl. *J. Fluid Mech.*, **96**, 769

Ramos, J. I. and Somer, H. T. 1985. Swirling flows in a research combustor. *AIAA J.*, **23**, 241–248

Rohde, D. L., Lilley, D. G., and McLaughlin, D. K. 1983. Mean flow fields in axisymmetric combustor geometries with swirl. *AIAA J.*, **21**, 593–600

Sislian, J. P. and Cusworth, R. A. 1986. Measurements of mean velocity and turbulent intensities in a free isothermal jet. *AIAA J.*, **24**, 303–309

Synder, P. K., Orloff, L. K., and Reinath, M. S. 1984. Reduction of flow measurements uncertainties in laser velocimeters with non-orthogonal channels. *AIAA J.*, **22**, 1115–1123

Syred, N., Chigier, N. A., and Beer, J. M. 1971. Turbulence measurements in swirling recirculating flows. Symposium on Internal Flows, University of Salford, Paper 13, B27

Vu, B. T. and Gouldin, F. C. 1982. Flow measurements in a model swirl combustor. *AIAA J.*, **20**, 642–651